Physica B 685 (2024) 416057

Contents lists available at ScienceDirect

Physica B: Condensed Matter

journal homepage: www.elsevier.com/locate/physb

Hydrostatic pressure and temperature dependent optical properties of double inverse parabolic quantum well under the magnetic field

A. Shaer [a], M.B. Yücel [b], E. Kasapoglu [c,*]

[a] College of Sciences, An-Najah National University, Physics Department, 400 Nablus, Palestine
[b] Akdeniz University, Science Faculty, Physics Department, 07058, Antalya, Turkey
[c] Sivas Cumhuriyet University, Science Faculty, Physics Department, 58140, Sivas, Turkey

ARTICLE INFO

Keywords:
Double inverse parabolic quantum well
Nonlinear absorption
Hydrostatic pressure
Temperature
Magnetic field

ABSTRACT

In this study, we investigated the combined effects of structure parameters such as size and geometry, as well as hydrostatic pressure, temperature, and magnetic field on the electronic and optical properties of a double inverse parabolic quantum well within the framework of the effective mass and parabolic band approximations. It is very important to consider the effects of temperature and hydrostatic pressure, especially in practical applications involving quantum wells such as semiconductor devices and optoelectronics. The results obtained are in good agreement with the literature. Understanding how these factors affect the electronic and optical properties of semiconductor heterostructures helps to optimize the performance and stability of devices operating under different environmental conditions.

1. Introduction

As known, there is considerable interest in the optical phenomena based on low-dimensional systems which have different shapes and sizes in the presence of external perturbations such as intense laser field, electric field, magnetic field, hydrostatic pressure and temperature [1–17]. All of the provided results indicate that the various factors such as temperature, applied electric and magnetic field, and hydrostatic pressure affect the electronic and optical properties of these semiconductor materials. Particularly, the manipulation of hydrostatic pressure leads to change in the confinement of electrons and in different transitions, which is very useful to fabricated optoelectronics devices. It is because the band gap of the material can be tuned and thereby the change in property may be applied for electronic and optoelectronic devices. It is very important to consider the effects of temperature and hydrostatic pressure, especially in practical applications involving quantum wells such as semiconductor devices and optoelectronics. Understanding how these factors affect electronic and optical properties helps to optimize the performance and stability of devices operating under different environmental conditions. In particular, by means of the applied hydrostatic pressure, one may generate indirect transitions in the energy-space. These transitions come from the appearance of the hydrostatic pressure-induced conduction band minimum at the X point of the Brillouin zone of the materials that make up the potential barriers. The combined effect of the temperature, and hydrostatic pressure is a good tool to modify the effective mass of the electron, band structure, confinement potential, as well as dielectric constant and they lead to a modification in the property of elementary excitation in heterostructures [18,19].

The possibility of experimentally producing an inverse parabolic quantum well makes [20,21] it worth studying. In this study, we put forward the effects of external magnetic field, hydrostatic pressure, temperature, and structural parameters defining the confinement potential on the electronic and optical properties of AlGaAs/GaAs double inverse parabolic quantum well (DIPQW). The organization of the work is as following: Section 2 includes the theoretical model. Section 3 includes results and discussion. Finally, Section 4 contains the main conclusions of the study.

2. Theory

In the effective mass approximation, the Hamiltonian for DIPQW as a function of the hydrostatic pressure and temperature under the magnetic field is as follows

$$H = \frac{1}{2m^*(P,T)}\left[\vec{p} + \frac{e}{c}\vec{A}(\vec{r})\right]^2 + V(z,P,T) \quad (1)$$

* Corresponding author.
E-mail address: ekasap@cumhuriyet.edu.tr (E. Kasapoglu).

https://doi.org/10.1016/j.physb.2024.416057
Received 20 March 2024; Received in revised form 16 April 2024; Accepted 29 April 2024
Available online 30 April 2024
0921-4526/© 2024 Elsevier B.V. All rights reserved.

where $\vec{p}$ is the momentum of the electron, $\vec{A}(\vec{r})$ is the vector potential of the magnetic field, the magnetic field is applied perpendicular to the growth direction (z-direction), i. e., magnetic field and vector potential have the forms of $\vec{B} = (B, 0, 0)$ and $\vec{A} = (0, Bz, 0)$, e is the elementary charge, c is the speed of light.

The hydrostatic pressure and temperature dependent effective mass for the electron is given by [22–25].

$$m^*(P,T) = \frac{m_0}{1 + E_p^{\Gamma}\left[\frac{2}{E_g^{\Gamma}(P,T)} + \frac{1}{E_g^{\Gamma}(P,T)+\Delta_0}\right]} \tag{2}$$

where m_0 is the free electron mass, $E_p^{\Gamma} = 7.51$ eV, $\Delta_0 = 0.341$ eV and $E_g^{\Gamma}(P,T)$ is the hydrostatic pressure and temperature dependent energy gap for the GaAs quantum well at the Γ-point in the units of eV. It is given by [26,27]

$$E_g^{\Gamma}(P,T) = E_g^{\Gamma}(0,T) + 1.26 \times 10^{-2} P - 3.77 \times 10^{-5} P^2 \tag{3}$$

where $E_g^{\Gamma}(0,T) = 1.519 - (5.405 \times 10^{-4} T^2)/(T + 204)$eV.

The hydrostatic pressure in the unit of kbar and the temperature in the unit of Kelvin (K) dependent static dielectric constant is given by [26,27].

$$\varepsilon(P,T) = \begin{cases} (i)\ 12.74\, e^{-1.73\times10^{-3}P}\ e^{9.4\times10^{-5}(T-75.6)}\ ; & \text{for } T < 200\ \text{K}, \\ (ii)\ 13.18\, e^{-1.73\times10^{-3}P}\ e^{20.4\times10^{-5}(T-300)}\ ; & \text{for } T \geq 200\ \text{K}, \end{cases} \tag{4}$$

where the charge image effects have not been considered (i.e. $\varepsilon_w(P,T) = \varepsilon_b(P,T)$).

In Eq. (1), $V(z,P,T)$ is the DIPQW potential that confines the electron, the functional expression of the potential as a function of position, pressure and temperature is given as follows

$$V(z,P,T) = \begin{cases} -\dfrac{4V_o(P,T)}{\sigma\, L_w^2(P)}\left(L_b\,(P)/2 - |z|\right)\left(L_w(P) + L_b\,(P)/2 - |z|\right), & L_b \Big/ 2 \leq |z| \leq (L_{w+}L_b/2) \\ V_o\,(P,T), & elsewhere \end{cases} \tag{5}$$

where z represents the growth direction of the quantum well, $V_o(P,T)$ is the temperature and hydrostatic pressure dependent finite barrier height, $\sigma\ (= x_{max}/x_c)$ is the ratio of the aluminum concentration in the barrier region ($x_{max} = 0.3$) to that in the well center (x_c), $L_w(P)$ and $L_b(P)$ are the temperature and hydrostatic pressure dependent well and barrier widths. The variations of the well and barrier widths with hydrostatic pressure are given by [28–30]

$$\begin{aligned} L_w(P) &= L_{w0}(1 - (S_{11} + 2S_{12})P) \\ L_b(P) &= L_{b0}(1 - (S_{11} + 2S_{12})P) \end{aligned} \tag{6}$$

where L_{w0} (L_{b0}) is the well (barrier) width in the zero hydrostatic pressure, $S_{11} = 1.16x10^{-3} kbar^{-1}$ and $S_{12} = -3.7x10^{-4} kbar^{-1}$ are the elastic for GaAs material. The barrier height is given by [31,32]

$$V_0(P,T) = Q_c \Delta E_g^{\Gamma}(x,P,T) \tag{7}$$

where $Q_c (= 0.6)$ is the conduction band offset parameter, x is the mole fraction of aluminum in $Ga_{1-x}Al_xAs$ layer, and $\Delta E_g^{\Gamma}(x,P,T)$ is the band gap difference between quantum well and the barrier matrix at the Γ-point as a function of hydrostatic pressure and temperature.

In order to solve Eq. (1), we used the diagonalization method by choosing orthonormal base functions that are solutions of an infinite square quantum well with L-width. L is infinite well width at the far end of QW which is large enough when compared with the quantum well width which is considered. The $L-$ value is determined according to the convergence of the energy eigenvalues. The bases are formed as follows [33]:

$$\varphi_n(z) = \sqrt{\frac{2}{L}} cos\left(\frac{n\pi z}{\mathrm{L}} - \delta_n\right), \tag{8}$$

where δ_n is

$$\delta_n = \begin{cases} 0, n\ is\ odd \\ \dfrac{\pi}{2}, n\ is\ even \end{cases}, \tag{9}$$

and so, the wave function in the z-direction is expanded in a set of basis functions as follows

$$\psi(z) = \sum_{n=1}^{N} c_n \varphi_n(z), \tag{10}$$

where N is the size of the matrix. When calculating the wave function $\psi(z)$, we ensured that the eigenvalues are independent of the chosen infinite quantum well width $- L$, and the wave functions are localized in the well region. This method requires embedding any well potential into an infinite square well, whose presence of the confining walls has no effect on the solutions. The width of the infinite square well has been chosen large enough so that the solutions are not sensitive to infinite walls. Further, the size of the matrix (the upper limit$-N$ of the sum in Eq. (10)) is increased until convergence to any desired accuracy is achieved. It should be noted that in this study, the value of N is chosen large enough to guarantee a precise accuracy also for all confined states in different types of quantum wells considered. For example, $N = 50$ was large enough to guarantee accuracy down to 0.1 meV for all bound states, ensuring that the effects of infinite potential barriers on the energies of bounded states were negligible and that precision at the energy of 0.1 meV was maintained.

Immediately after the energies and related wavefunctions are acquired, linear, third-order nonlinear and total absorption coefficients (TAC) are found for transitions between any two electronic states by using the perturbation expansion and the density matrix methods [2,4, 31–35], respectively

$$\beta^{(1)}(\omega) = \sqrt{\frac{\mu_o}{\varepsilon_r}}\ \frac{\left|M_{ij}\right|^2 \sigma_v \hbar\omega\ \Gamma_{ij}}{\left(E_{ij} - \hbar\omega\right)^2 + \left(\hbar\Gamma_{ij}\right)^2}, \tag{11}$$

$$\begin{aligned} \beta^{(3)}(\omega, I) = -2\sqrt{\frac{\mu_o}{\varepsilon_r}}\left(\frac{I}{\varepsilon_o n_r c}\right)\ \frac{\left|M_{ij}\right|^4 \sigma_v \hbar\omega\ \Gamma_{ij}}{\left[\left(E_{ij} - \hbar\omega\right)^2 + \left(\hbar\Gamma_{ij}\right)^2\right]^2} \\ \left(1 - \frac{\left|M_{jj} - M_{ii}\right|^2}{\left|2M_{ij}\right|^2}\ \frac{\left(E_{ij} - \hbar\omega\right)^2 - \left(\hbar\Gamma_{ij}\right)^2 + 2E_{ij}\left(E_{ij} - \hbar\omega\right)}{E_{ij}^2 + \left(\hbar\Gamma_{ij}\right)^2}\right), \end{aligned} \tag{12}$$

$$\beta(\omega, I) = \beta^{(1)}(\omega) + \beta^{(3)}(\omega, I), \tag{13}$$

where, $\varepsilon_r = n_r^2 \varepsilon_0$ is the real part of the permittivity, $n_r = \sqrt{\varepsilon}$ (depending on the temperature value, the ε-value in (i) or (ii) of Eq. (4) is used), σ_V is the carrier density in the system, μ_o is the vacuum permeability, $E_{ij} = E_j - E_i$ is the energy difference between two energy levels of the

electron, $M_{ij} = |\langle\psi_i|e\,z|\psi_j\rangle|, (i,j = 1,2)$ is the transition matrix element between the eigenstates ψ_i and ψ_j for incident radiation polarized in the z-direction, $\Gamma_{ij}(= 1/T_{ij})$ is the relaxation rate, T_{ij} is the relaxation time, c is the speed of the light in free space, and I is the intensity of incident photon with the ω-angular frequency that leads to the intersubband optical transitions. It should be noted that diagonal dipole matrix elements are zero ($M_{ii} = M_{jj} = 0$), and non-diagonal ones are different zero ($M_{ij} \neq 0$) due to the symmetric character of DIPQW potential.

3. Results and discussions

The parameter values in our numerical calculations are $\varepsilon_o = 8.85x10^{-12}C^2N^{-1}m^{-2}$, $T_{12} = 0.4\,ps$, $\Gamma_{12} = 1/T_{12}$, $\mu_o = 4\pi\,x10^{-7}Hm^{-1}$, $\sigma_v = 3.0x10^{22}\,e/m^3$ and $I = 1.0x10^8\,W/m^2$. These parameters are suitable for GaAs/GaAlAs heterostructures [33–35].

The squared ground state wave function and potential profile confining of the electron in a double quantum well with each well having an inverse parabolic shape with a well width of $L_w = 10\,nm$ and the barrier width of $L_b = 2.5\,nm$ for different σ-values ($\sigma = 1.5$ and $\sigma = 2.0$) in the absence and presence of the magnetic field are given in Fig. 1 (a) and (b), respectively. As the value of parameter-σ causes a decrease

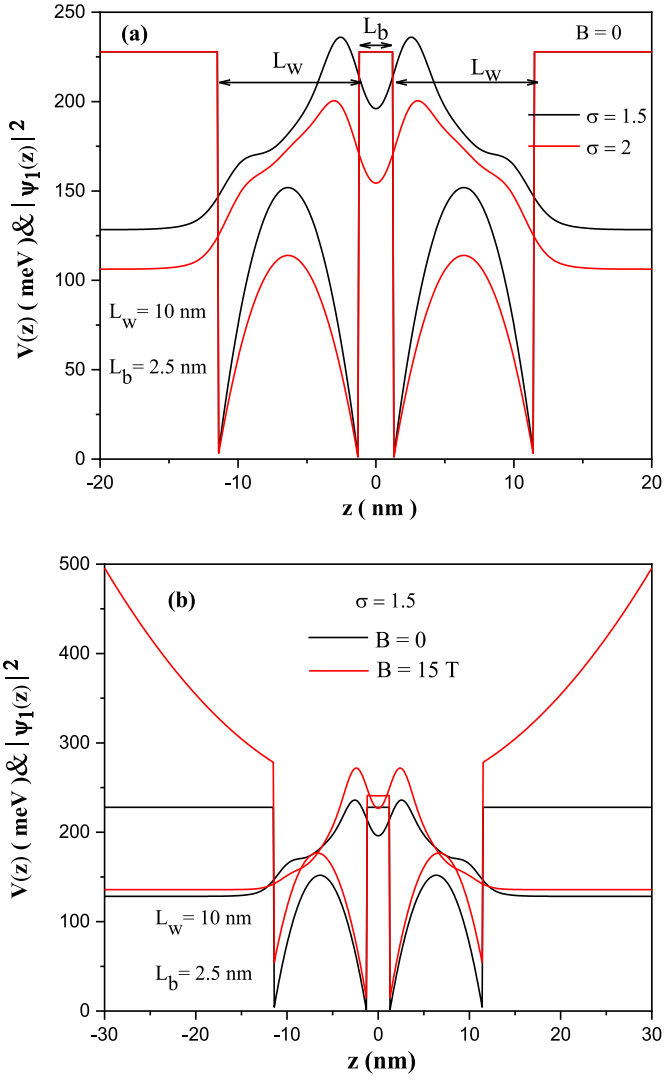


Fig. 1. For different σ-values ($\sigma = 1.5$ and $\sigma = 2.0$), the squared ground state wave function and potential profile confining of the electron in a double inverse parabolic quantum well which has the well and barrier widths $L_w = 10\,nm$ and $L_b = 2.5\,nm$, respectively: (a) $B = 0$ and (b) $B = 15\,T$.

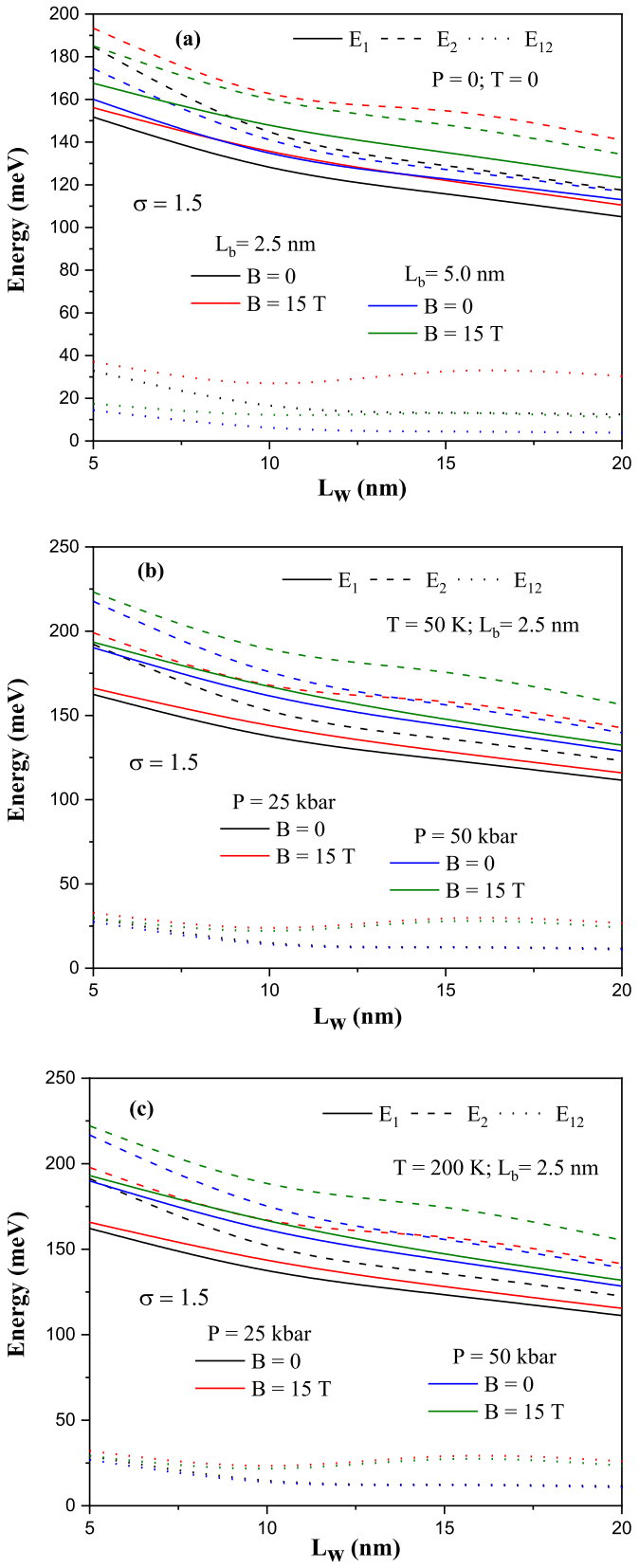


Fig. 2. For $\sigma = 1.5$, in the absence and presence of the magnetic field the variation of ground (solid lines) and first excited (dashed lines) energies and energy difference (dotted lines) between these energy levels as a function of the well width: for different barrier widths ($L_b = 2.5\,nm$ and $L_b = 5.0\,nm$) (a) $P = 0$ and $T = 0$, for different two hydrostatic pressure values ($P = 25\,kbar$ and $P = 50\,kbar$) (b) $T = 50\,K$ and (c) $T = 200\,K$.

in energy due to the decrease in the peak height of the dome at the center of the well, which we call the inverse parabola, the magnetic field causes an increase in energies since it provides extra parabolic confinement for the electron.

For $\sigma = 1.5$, in the absence and presence of the magnetic field the variation of ground (solid lines) and first excited (dashed lines) energies and energy difference (dotted lines) between these energy levels as a function of the well width are given in Fig. 2(a–c). In Fig. 2 (a), given results are for two different barrier widths ($L_b = 2.5\,nm$ and $L_b = 5.0\,nm$) as independent of the hydrostatic pressure and temperature. In Fig. 2 (b) and (c), for $L_b = 2.5\,nm$ and two different hydrostatic pressure values ($P = 25\,kbar$ and $P = 50\,kbar$), the given results are for the temperature values of $T = 50\,K$ and $T = 200\,K$, respectively.

Fig. 3(a–c) has the same regulation as Fig. 2(a–c), but it is for $\sigma = 2.0$. In the absence and presence of hydrostatic pressure, temperature and magnetic field, common results for both figures are those: energies and energy differences are decreasing functions of the well dimensions depending on increasing effective length-L_{eff} ($= L_w + L_b + L_w$). The energies and energy differences are decreasing functions of hydrostatic pressure. As the hydrostatic pressure increases, the dielectric constant, depth of wells, and effective mass of electrons increase, leading to more electron confinement. Thus the sub-band energies of electrons increase for all well dimensions, while the energy difference between any two energy levels decreases with the hydrostatic pressure. The energies and energy differences are increasing functions of the magnetic field since the magnetic field provides an extra parabolic confinement for electrons. The increment in energy due to the hydrostatic pressure is lower than that due to the magnetic field. Since temperature causes only a minimal increase in the dielectric constant and the effective mass of the electron, it causes a decrease in the energies and the energy difference between the relevant energy levels. This decrement is lower than the decrement in the hydrostatic pressure effect.

For $\sigma = 1.5$, in the absence and presence of the hydrostatic pressure, temperature, and magnetic field effects the change results on the total absorption peaks corresponding to the (1–2) transition of an electron in DIPQW for two different well widths ($L_w = 10\,nm$ and $L_w = 20\,nm$) and barrier widths ($L_b = 2.5\,nm$ and $L_b = 5.0\,nm$) versus the resonant photon energy are given in Fig. 4(a–c). The results in Fig. 4 (a) are independent hydrostatic pressure and temperature and the results in Fig. 4 (b) and (c) are for temperature values of $T = 50\,K$ and $T = 200\,K$ for only $L_b = 2.5\,nm$ and two different hydrostatic pressure values ($P = 25\,kbar$ and $P = 50\,kbar$), respectively. Solid lines (dashed lines) are for $B = 0$ ($B = 15\,T$). In Fig. 4 (a), when there is no hydrostatic pressure and temperature effects, absorption peak positions shift towards the red with decreasing amplitudes due to a decrease in the energy difference between the first two electronic levels of interest with increasing the well and barrier widths or effective length. Due to the increase in the energy difference with the effect of the magnetic field, absorption peak positions shift towards the blue with increasing amplitudes. The results in Fig. 4 (b) and (c) are for only a single barrier width ($L_b = 2.5\,nm$). In the direction of the changes in energies caused by hydrostatic pressure and temperature effects in Fig. 2, the absorption peak positions shift towards the red with decreasing amplitudes. At the same hydrostatic pressure values, an additional increase in temperature causes this behavior to continue, but it is not very pronounced.

The arrangements in Fig. 5(a–c) are exactly as in Fig. 4(a–c), but the results are for $\sigma = 2.0$. As explained earlier, since the parameter-σ also causes a weakening of the geometric confinement, the position of the absorption peaks shifts towards the red. The peak amplitudes decrease for $L_w = 10\,nm$ and increase for $L_w = 20\,nm$ both in the absence and presence of the magnetic field. In Fig. 5 (a), the total absorption peak given by the green line is divided into two peaks which is known as the bleaching effect. This effect occurs when the energy difference between the levels considered is quite small and the light intensity that provides the transition between these sub-bands remains quite large for this

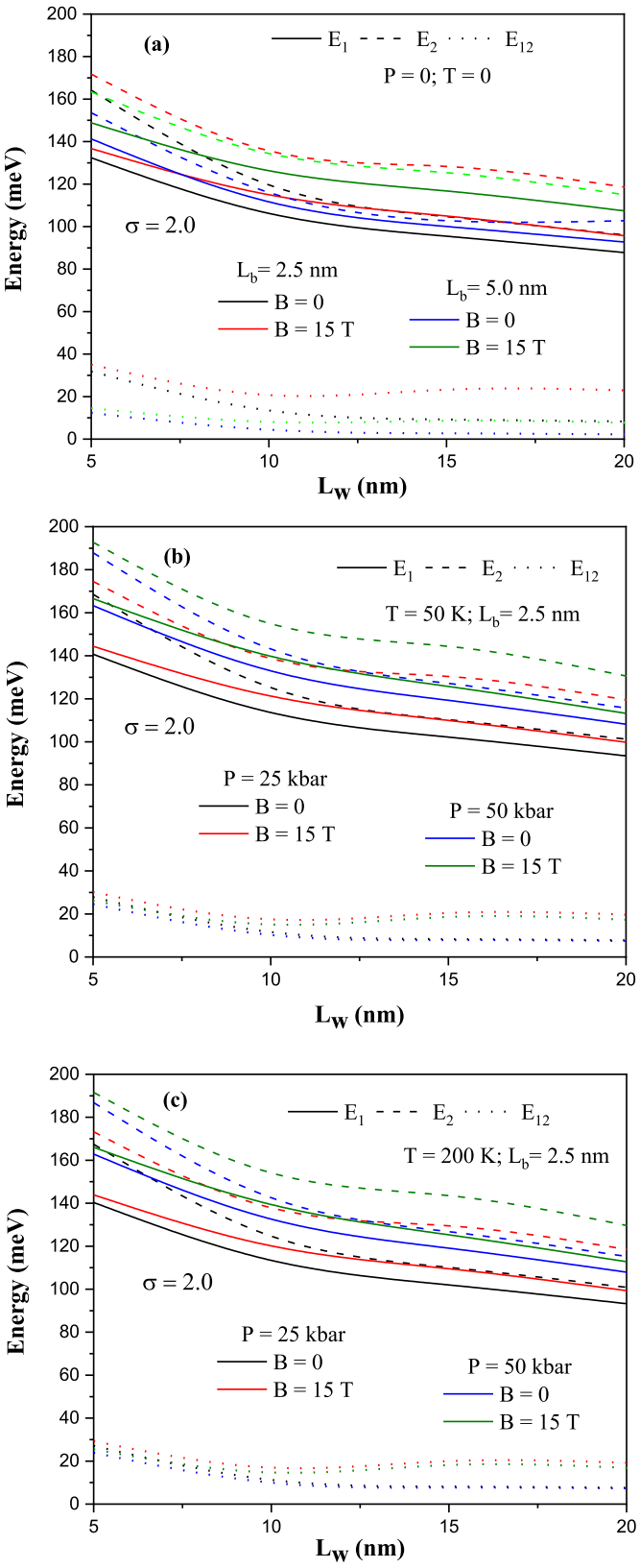


Fig. 3. For $\sigma = 2.0$, in the absence and presence of the magnetic field the variation of ground (solid lines) and first excited (dashed lines) energies and energy difference (dotted lines) between these energy levels as a function of the well width: for different barrier widths ($L_b = 2.5\,nm$ and $L_b = 5.0\,nm$) (a) $P = 0$ and $T = 0$, for different two hydrostatic pressure values ($P = 25\,kbar$ and $P = 50\,kbar$) (b) $T = 50\,K$ and (c) $T = 200\,K$.

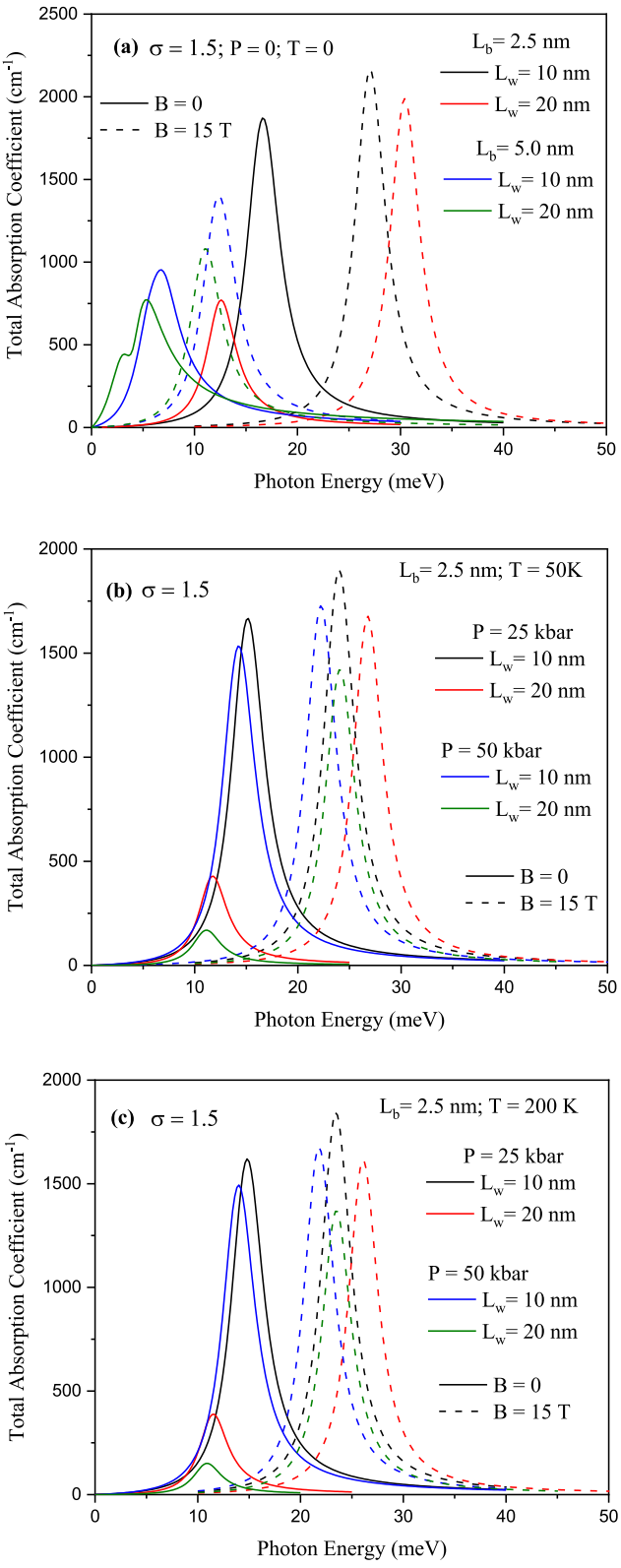


Fig. 4. For $\sigma = 1.5$, the variation of total absorption peaks corresponding to the (1–2) transition of an electron in double inverse parabolic quantum well for two different well widths ($L_w = 10\,nm$ and $L_w = 20\,nm$) as a function of the resonant photon energy: for different barrier widths ($L_b = 2.5\,nm$ and $L_b = 5.0\,nm$), (a) $P = 0$ and $T = 0$, for different two hydrostatic pressure values ($P = 25\,kbar$ and $P = 50\,kbar$) (b) $T = 50\,K$ and (c) $T = 200\,K$. Solid lines (dashed lines) are for $B = 0$ ($B = 15\,T$).

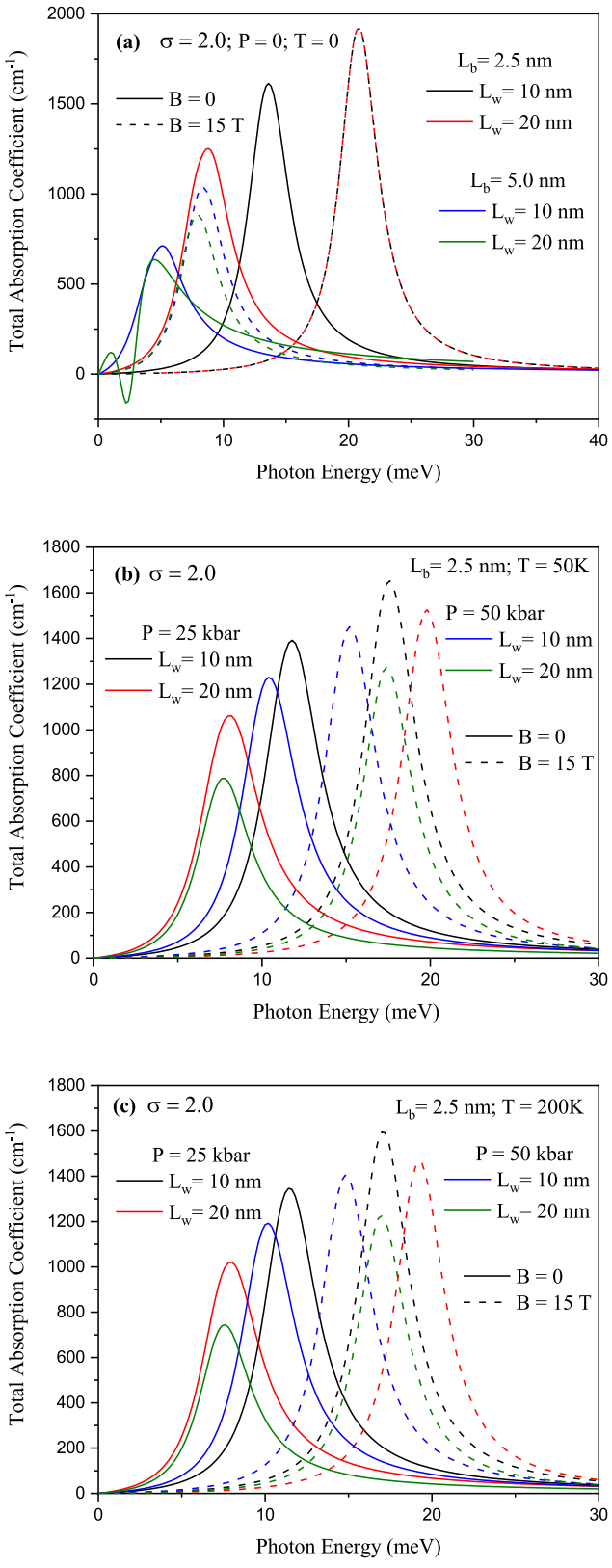


Fig. 5. For $\sigma = 2.0$, the variation of total absorption peaks corresponding to the (1–2) transition of an electron in double inverse parabolic quantum well for two different well widths ($L_w = 10\,nm$ and $L_w = 20\,nm$) as a function of the resonant photon energy: for different barrier widths ($L_b = 2.5\,nm$ and $L_b = 5.0\,nm$), (a) $P = 0$ and $T = 0$, for different two hydrostatic pressure values ($P = 25\,kbar$ and $P = 50\,kbar$) (b) $T = 50\,K$ and (c) $T = 200\,K$. Solid lines (dashed lines) are for $B = 0$ ($B = 15\,T$).

energy difference. This effect can be eliminated by using lower light intensity or by increasing the energy difference between the levels of interest by changing external field effects and structure parameters for the same light intensity [32]. The reason why this effect cannot be observed in other peaks is that the energy difference between the levels to which these peaks belong is large enough. Usually, to explain the changes in the amplitudes of the ACs, the dipole matrix element are used since the linear term and third-order nonlinear terms of AC are proportional to $|M_{ij}|^2$ and $(|M_{ij}|^4$, respectively. However, in some cases, using the dipole matrix element alone is insufficient to explain the variations of the peak amplitudes. The energy difference-E_{ij} between the two levels of interest plays an effective role not only on the peak positions but also on the peak amplitudes. As known, resonance conditions for incident photon energy are satisfied with the equality $\hbar\omega_{\max} = \sqrt{(E_{ij}-\hbar\omega)^2+(\hbar\Gamma_{ij})^2}$ for which the linear AC has a maximum value, and so the maximum value of linear AC in Eq. (11) becomes directly proportional to the energy difference and squared dipole matrix element in the form of $|M_{ij}|^2(E_{ij}+\sqrt{(E_{ij}-\hbar\omega)^2+(\hbar\Gamma_{ij})^2})$. The energy difference between the two energy levels is the dominant term on the peak positions of the ACs and peak positions of ACs shift towards the higher (smaller) photon energies as the transition energy increases (decreases). By using the resonance condition in the form of $\hbar\omega_{min} = \frac{1}{3}(E_{ij}+\sqrt{(4E_{ij})^2+3(\hbar\Gamma_{ij})^2})$ for the incident photon energy that corresponds to the minimum value of third-order nonlinear AC, it is seen that nonlinear AC depends on the parameters of I-light intensity, $|M_{ij}|^4$, and energy difference-E_{ij}. Since the linear term (third-order nonlinear term) of AC is proportional to $|M_{ij}|^2$ ($|M_{ij}|^4$), to explain the changes in the amplitudes of the ACs are used the dipole matrix elements. The changes of the IDME according to external parameters for constant values of $L_b = 2.5\,nm$; $\sigma = 2.0$ and $T = 50\,K$ are given in Table 1.

Table 1
For $L_b = 2.5\,nm$; $\sigma = 2.0$ and $T = 50\,K$, in the absence and presence of the magnetic field squared reduced dipole matrix elements for the values of some well widths and hydrostatic pressures.

L (nm)	P (kbar)	B (T)	$(\eta_{12})^2$ $(nm)^2$	E_{12} (meV)
10	0	0	34.8982	13.3982
	25	0	34.1309	11.5994
	50	0	33.4906	10.2102
	0	15	24.4134	20.6428
	25	15	24.4376	17.4723
	50	15	24.3726	15.1086
20	0	0	53.2657	8.298
	25	0	42.1534	7.75794
	50	0	27.3105	7.4638
	0	15	20.0984	22.8402
	25	15	19.0016	19.7026
	50	15	17.4569	17.3196

4. Conclusion

In this study, we investigated the combined effects of structure parameters such as size and geometry, as well as hydrostatic pressure, temperature, and magnetic field on the electronic and optical properties of GaAs/GaAlAs double inverse parabolic quantum well. Hydrostatic pressure causes an increase in well depth and effective mass of the electron, and a decrease in dielectric constant, the well and barrier widths. Temperature only causes an increase in the dielectric constant and the effective mass of the electron. The effect of these two factors causes the absorption peaks to move towards lower photon energies. Since the magnetic field provides a parabolic confinement in addition to the geometric confinement, it causes the absorption peaks to shift towards higher photon energies. The results obtained are in good agreement with the literature [36,37]. Thus, using the competitive effects of hydrostatic pressure, temperature and the magnetic field, the electronic and optical properties of materials can be tuned to aim. In this context, temperature and hydrostatic pressure variations can impact the stability and reliability of devices. Accounting for these effects ensures that devices maintain their functionality and performance even when exposed to varying environmental conditions and more accurate models and the development of more robust and reliable technologies. Pressure-induced changes affect the bandgap of the semiconductors, energy levels, and effective masses of charge carriers. Since temperature affects the thermal energy of electrons and phonons in quantum wells, electron-phonon interactions become more pronounced, leading to broadening of energy levels and enhancement of scattering processes. The combined effects of pressure and temperature can also influence the interband and intraband transitions, leading to shifts in the peak wavelengths and changes in the optical response of quantum wells. Understanding the interplay between hydrostatic pressure and temperature is crucial for tailoring the optical properties of quantum wells for various applications, such as optoelectronic devices, sensors, and quantum information processing.

CRediT authorship contribution statement

A. Shaer: Writing – review & editing, Validation, Conceptualization. **M.B. Yücel:** Validation, Software, Formal analysis, Conceptualization. **E. Kasapoglu:** Writing – review & editing, Writing – original draft, Validation, Conceptualization.

Declaration of competing interest

The authors declare that they have no known competing financial interests or personal relationships that could have appeared to influence the work reported in this paper.

Data availability

Data will be made available on request.

References

[1] M. Karimi, A. Keshavarz, Second harmonic generation in asymmetric double semi-parabolic quantum wells: effects of electric and magnetic fields, hydrostatic pressure and temperature, Phys. E Low-dimens. Syst. Nanostruct. 44 (9) (2012) 1900–1904, https://doi.org/10.1016/j.physe.2012.05.011.
[2] M. Nazari, M. Karimi, A. Keshavarz, Linear and nonlinear optical absorption coefficients and refractive index changes in modulation-doped quantum wells: effects of the magnetic field and hydrostatic pressure, Phys. B Condens. Matter 428 (2013) 30–35, https://doi.org/10.1016/j.physb.2013.07.015.
[3] J.C. Martínez-Orozco, M.E. Mora-Ramos, C.A. Duque, Nonlinear optical rectification and second and third harmonic generation in gaas δ-fet systems under hydrostatic pressure, J. Lumin. 132 (2) (2012) 449–456, https://doi.org/10.1016/j.jlumin.2011.09.022.
[4] J.C. Martínez-Orozco, M.E. Mora-Ramos, C.A. Duque, The nonlinear optical absorption and corrections to the refractive index in a gaas n-type delta-doped field effect transistor under hydrostatic pressure, Phys. Status Solidi 249 (1) (2012) 146–152, https://doi.org/10.1002/pssb.201147301.
[5] A.J. Peter, Navaneethakrishnan, Simultaneous effects of pressure and temperature on donors in a gaalas/gaas quantum well, Superlattice. Microst. 43 (1) (2008) 63–71, https://doi.org/10.1016/j.spmi.2007.06.007.
[6] C. Duque, M. Mora-Ramos, M. Barseghyan, Electronic states in a pöschl–teller-like quantum well: combined effects of electric field, hydrostatic pressure, and temperature, Superlattice. Microst. 50 (5) (2011) 480–490, https://doi.org/10.1016/j.spmi.2011.08.010.
[7] Z.-H. Zhang, L. Zou, K.-X. Guo, J.-H. Yuan, The effect of hydrostatic pressure, temperature and magnetic field on the nonlinear optical properties of asymmetrical Gaussian potential quantum wells, Phys. E Low-dimens. Syst. Nanostruct. 77 (2016) 90–96, https://doi.org/10.1016/j.physe.2015.11.012.
[8] N.T.X. Hoai, N.D. Hien, Magneto-optical transport properties of parabolic potential gaas/ga1− κalκas wells under the influence of al concentration and hydrostatic pressure, Phys. E Low-dimens. Syst. Nanostruct. 127 (2021) 114491, https://doi.org/10.1016/j.physe.2020.114491.
[9] E. Kasapoglu, F. Ungan, H. Sari, I. Sökmen, The hydrostatic pressure and temperature effects on donor impurities in cylindrical quantum wire under the magnetic field, Phys. E Low-dimens. Syst. Nanostruct. 42 (5) (2010) 1623–1626, https://doi.org/10.1016/j.physe.2010.01.009.

[10] E. Kasapoglu, The hydrostatic pressure and temperature effects on donor impurities in gaas/ga1− xalxas double quantum well under the external fields, Phys. Lett. 373 (1) (2008) 140–143, https://doi.org/10.1016/j.physleta.2008.10.080.
[11] S. Liang, W. Xie, The hydrostatic pressure and temperature effects on a hydrogenic impurity in a spherical quantum dot, Eur. Phys. J. B 81 (2011) 79–84, https://doi.org/10.1140/epjb/e2011-10831-9.
[12] Y. Naimi, A. Jafari, Optical properties of quantum dots versus quantum antidots: effects of hydrostatic pressure and temperature, J. Comput. Electron. 13 (3) (2014) 666–672, https://doi.org/10.1007/s10825-014-0585-9.
[13] M. Narayanan, A.J. Peter, Pressure and temperature induced non-linear optical properties in a narrow band gap quantum dot, Quantum Matter 1 (1) (2012) 53–58, https://doi.org/10.1166/qm.2012.1005.
[14] A. Bera, M. Ghosh, Simultaneous influence of hydrostatic pressure and temperature on binding energy of impurity doped quantum dots in presence of noise, J. Alloys Compd. 695 (2017) 3054–3060, https://doi.org/10.1016/j.jallcom.2016.11.345.
[15] P. Silotia, K. Batra, V. Prasad, Asymmetric effects on the optical properties of double-quantum well systems, Opt. Eng. 53 (2) (2014), https://doi.org/10.1117/1.OE.53.2.027105, 027105-027105.
[16] V. Prasad, B. Dahiya, Modifications of laser field assisted intersubband transitions in the coupled quantum wells due to static electric field, Phys. Status Solidi 248 (7) (2011) 1727–1734, https://doi.org/10.1002/pssb.201046582.
[17] B. Dahiya, V. Prasad, K. Yamashita, Dynamics of intersubband transitions in triangular quantum wells due to static magnetic and laser fields, J. Lumin. 136 (2013) 240–248, https://doi.org/10.1016/j.jlumin.2012.11.041.
[18] E. Reyes-Gómez, N. Raigoza, L. Oliveira, Effects of hydrostatic pressure and aluminum concentration on the conduction-electron g factor in gaas-(ga,al) as quantum wells under in-plane magnetic fields, Phys. Rev. B 77 (11) (2008) 115308, https://doi.org/10.1103/PhysRevB.77.115308.
[19] N. Raigoza, C. Duque, E. Reyes-Gómez, L. Oliveira, Hydrostatic-pressure effects on the correlated electron–hole transition energies in gaas–ga1–xalxas semiconductor quantum wells, Phys. Status Solidi 243 (3) (2006) 635–640, https://doi.org/10.1002/pssb.200541303.
[20] W. Chen, S. Wang, T. Andersson, J. Thordson, Inverse parabolic quantum wells grown by molecular-beam epitaxy using digital and analog techniques, Phys. Rev. B 48 (19) (1993) 14264, https://doi.org/10.1103/PhysRevB.48.14264.
[21] W. Chen, S. Wang, T. Andersson, J. Thordson, Inverse parabolic quantum well and its quantum-confined Stark effect, J. Appl. Phys. 74 (10) (1993) 6247–6250, https://doi.org/10.1063/1.355167.
[22] A. Sali, H. Satori, The combined effect of pressure and temperature on the impurity binding energy in a cubic quantum dot using the fem simulation, Superlattice. Microst. 69 (2014) 38–52, https://doi.org/10.1016/j.spmi.2014.01.011.
[23] K. El-Bakkari, A. Sali, E. Iqraoun, A. Rezzouk, N. Es-Sbai, M.O. Jamil, Effects of the temperature and pressure on the electronic and optical properties of an exciton in gaas/ga1− xalxas quantum ring, Phys. B Condens. Matter 538 (2018) 85–94, https://doi.org/10.1016/j.physb.2018.03.010.
[24] H. Ehrenreich, Band structure and transport properties of some 3–5 compounds, J. Appl. Phys. 32 (10) (1961) 2155–2166, https://doi.org/10.1063/1.1777035.
[25] B. Welber, M. Cardona, C. Kim, S. Rodriguez, Dependence of the direct energy gap of gaas on hydrostatic pressure, Phys. Rev. B 12 (12) (1975) 5729, https://doi.org/10.1103/PhysRevB.12.5729.
[26] E. Niculescu, N. Eseanu, Hydrostatic pressure and electric field effects on the normalized binding energy in asymmetrical quantum wells, Eur. Phys. J. B 75 (2010) 247–251. http://hdl.handle.net/10.1140/epjb/e2010-00149-7.
[27] G.A. Samara, Temperature and pressure dependences of the dielectric constants of semiconductors, Phys. Rev. B 27 (6) (1983) 3494, https://doi.org/10.1103/PhysRevB.27.3494.
[28] E. Kasapoglu, H. Sari, I. Sokmen, Shallow donor impurities in different shaped double quantum wells under the hydrostatic pressure and applied electric field, Phys. B Condens. Matter 362 (1–4) (2005) 56–61, https://doi.org/10.1016/j.physb.2005.01.475.
[29] S. Adachi, Gaas, alas, and al x ga1− x as: material parameters for use in research and device applications, J. Appl. Phys. 58 (3) (1985) R1–R29, https://doi.org/10.1063/1.336070.
[30] R. Kopf, M. Herman, M.L. Schnoes, A. Perley, G. Livescu, M. Ohring, Band offset determination in analog graded parabolic and triangular quantum wells of gaas/algaas and gainas/alinas, J. Appl. Phys. 71 (10) (1992) 5004–5011, https://doi.org/10.1063/1.350600.
[31] A. Ed-Dahmouny, A. Sali, N. Es-Sbai, R. Arraoui, C. Duque, The impact of hydrostatic pressure and temperature on the binding energy, linear, third-order nonlinear, and total optical absorption coefficients and refractive index changes of a hydrogenic donor impurity confined in gaas/al x ga1− x as double quantum dots, The European Phys. J. Plus 137 (7) (2022) 784, https://doi.org/10.1140/epjp/s13360-022-03002-0.
[32] I. Karabulut, M. Mora-Ramos, C. Duque, Nonlinear optical rectification and optical absorption in gaas–ga1–xalxas asymmetric double quantum wells: combined effects of applied electric and magnetic fields and hydrostatic pressure, J. Lumin. 131 (7) (2011) 1502–1509, https://doi.org/10.1016/j.jlumin.2011.03.044.
[33] H. Dakhlaoui, W. Belhadj, E. Kasapoglu, F. Ungan, Position-dependent-mass and laser field impact on the optical characteristics of Manning-like double quantum well, Phys. E Low-dimens. Syst. Nanostruct. 151 (2023) 115737, https://doi.org/10.1016/j.physe.2023.115737.
[34] P. Silotia, Engineering optical properties of double quantum well systems, Indian J. Pure Appl. Phys. 54 (10) (2016) 641–650, https://doi.org/10.56042/ijpap.v54i10.9210.
[35] E. Kasapoglu, M. Yücel, C. Duque, Electronic and optical properties of the exponential and hyperbolic rosen–morse types quantum wells under applied magnetic field, The European Phys. J. Plus 138 (11) (2023) 1026, https://doi.org/10.1140/epjp/s13360-023-04594-x.
[36] F. Ungan, U. Yesilgul, S. Sakiroglu, M. Mora-Ramos, C. Duque, E. Kasapoglu, H. Sari, I. Sökmen, Simultaneous effects of hydrostatic pressure and temperature on the nonlinear optical properties in a parabolic quantum well under the intense laser field, Opt Commun. 309 (2013) 158–162, https://doi.org/10.1016/j.optcom.2013.07.006.
[37] M. Sayrac, H. Dakhlaoui, M. Mora-Ramos, F. Ungan, Hydrostatic pressure and temperature effects on nonlinear optical properties in harmonic-Gaussian asymmetric double quantum wells, Phys. Scripta 99 (4) (2024) 045942, https://doi.org/10.1088/1402-4896/ad3150.